blood® Regular Article

Check for updates

HEMATOPOIESIS AND STEM CELLS

Dopamine signaling regulates hematopoietic stem and progenitor cell function

Yang Liu,[1,2,*] Qi Chen,[1,2,*] Hyun-Woo Jeong,[1,2] Dong Han,[3] Jörg Fabian,[4] Hannes C.A. Drexler,[5] Martin Stehling,[6] Hans R. Schöler,[3] and Ralf H. Adams[1,2]

[1]Department of Tissue Morphogenesis, Max Planck Institute for Molecular Biomedicine, Muenster, Germany; [2]Faculty of Medicine, University of Münster, Muenster, Germany; [3]Department of Cell and Developmental Biology, Max Planck Institute for Molecular Biomedicine, Muenster, Germany; [4]Institute of Pharmaceutical and Medicinal Chemistry, University of Münster, Muenster, Germany; and [5]Mass Spectrometry Unit and [6]Flow Cytometry Unit, Max Planck Institute for Molecular Biomedicine, Muenster, Germany

KEY POINTS

- **Dopamine signaling influences hematopoietic stem cell maintenance, HSPC proliferation, and transplantation efficiency.**
- **Dopamine maintains Lck expression to control stem cell factor–induced ERK signaling downstream of c-Kit.**

Hematopoietic stem and progenitor cell (HSPC) function in bone marrow (BM) is controlled by stroma-derived signals, but the identity and interplay of these signals remain incompletely understood. Here, we show that sympathetic nerve–derived dopamine directly controls HSPC behavior through D_2 subfamily dopamine receptors. Blockade of dopamine synthesis, as well as pharmacological or genetic inactivation of D_2 subfamily dopamine receptors, leads to reduced HSPC frequency, inhibition of proliferation, and low BM transplantation efficiency. Conversely, treatment with a D_2-type receptor agonist increases BM regeneration and transplantation efficiency. Mechanistically, dopamine controls expression of the lymphocyte-specific protein tyrosine kinase (Lck), which, in turn, regulates MAPK-mediated signaling triggered by stem cell factor in HSPCs. Our work reveals critical functional roles of dopamine in HSPCs, which may open up new therapeutic options for improved BM transplantation and other conditions requiring the rapid expansion of HSPCs.

Introduction

Hematopoietic stem cells (HSCs) are indispensable for lifelong blood cell formation and, thereby, enable fundamental physiological processes, such as oxygen transport, immune responses, removal of debris, and tissue repair.[1–6] The maintenance and behavior of HSCs in bone marrow (BM) are regulated by niche microenvironments involving endothelial cells, vessel-associated reticular cells, adipocytes, and megakaryocytes.[1,2,7–19] Although some niche-derived signals, such as SCF and the chemokine Cxcl12, are well studied,[9,20–26] understanding of the microenvironmental control of HSC function remains incomplete.

Stroma-derived niche factors are also relevant for the challenged hematopoietic system. Chemotherapy or radiotherapy followed by BM transplantation, which are standard treatments for many hematopoietic malignancies, involve the rapid expansion of hematopoietic stem and progenitor cells (HSPCs).[1,2,8,14,24,25,27-31] Failure of these processes contribute to increased patient morbidity and mortality; thus, further insight into the signals controlling HSPCs is needed.[27,28,32]

Adrenergic nerves and noradrenaline secretion control circadian oscillations in HSC migration.[33–39] Adrenergic nerves in BM have been also associated with acute myelogenous leukemia, chemotherapy, and HSC ageing.[36,40-44] Adrenergic signals influence HSC behavior indirectly through alterations in niche cells,[42,45,46] whereas it is unclear whether sympathetic nerves control HSPCs directly.

The neuromodulator dopamine is synthesized from L-3, 4-dihydroxyphenylalanine, which, in turn, is generated from tyrosine by the enzyme tyrosine hydroxylase (Th).[47] Dopamine is essential in brain where dopaminergic neurotransmission regulates various behavioral traits and defective dopamine signaling is a cause of neurodegenerative disease.[48,49] Based on signaling activity, the 5 dopamine receptors can be divided into D_1-type (including Drd1 and Drd5) and D_2-type (Drd2, Drd3, and Drd4) receptors.[50]

Here, we show that dopamine signaling through D_2-type receptors regulates HSPC behavior in BM under steady-state conditions and after transplantation. We identify lymphocyte-specific protein tyrosine kinase (Lck) as a downstream target that is regulated by dopamine signaling and controls the response of HSPCs to extrinsic signals from the vascular niche.

Downloaded from http://ashpublications.net/blood/article-pdf/138/21/2051/1868550/bloodbld2020010419.pdf by guest on 29 May 2024

© 2021 by The American Society of Hematology

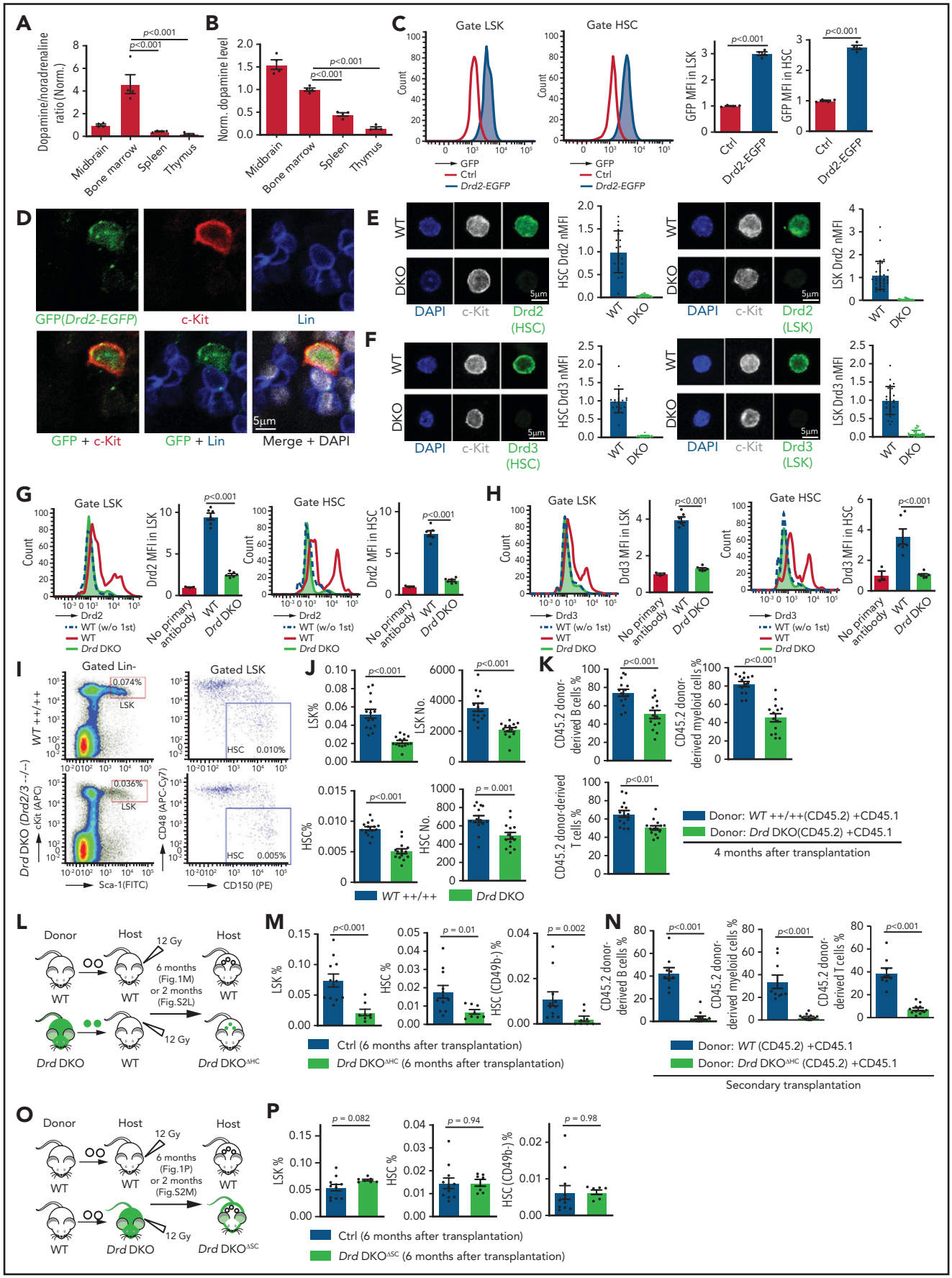

Figure 1.

Downloaded from http://ashpublications.net/blood/article-pdf/138/21/2051/1868550/bloodbld2020010419.pdf by guest on 29 May 2024

Methods

Mice

Th$^{tm1(Cre)Te}$ (*Th-Cre*),[51] *Rosa26-DTR*,[52] *Drd2*^{tm1Low},[53] *Drd3*^{tm1Dac},[54] *Rosa26-mTmG*,[55] *Vav1-Cre*,[56] *Wnt1-Cre*,[57] Lepr$^{tm2(cre)Rck}$,[58] and *Tg(Drd2-EGFP/Rpl10a)CP101Htz*[59] mice were used in this study.

FACS, immunostaining, and transplantation

Detailed descriptions of fluorescence-activated cell sorting (FACS), immunostaining, RNA sequencing (RNA-seq), pharmacological treatments, methylcellulose assays, lentiviral infections, quantitative polymerase chain reaction (qPCR) enzyme-linked immunosorbent assay (ELISA), mass spectrometry, and transplantation experiments are provided in supplemental Methods (available on the *Blood* Web site).

Results

D_2-type dopamine receptors cell autonomously regulate HSC maintenance

In a search for potential niche signals, we found that the normalized ratio and amount of dopamine in the extracellular fluid of BM are significantly higher relative to spleen and thymus (Figure 1A-B). Moreover, dopamine levels in BM are higher during the dark phase relative to daytime (supplemental Figure 1A). Dopamine may act directly on cells in marrow because bulk RNA-seq analysis of different BM cell types indicates that LSK (Lin$^-$ Sca-1$^+$ c-Kit$^+$) cells, which include HSPCs, express multiple dopamine receptors (supplemental Figure 1B).[15,21] This is consistent with a previous report showing dopamine receptor expression in CD34$^+$ human hematopoietic cells.[60] However, transcript levels of dopamine receptors are relatively low in LSK cells and in neurons, which are known to express these molecules (supplemental Figure 1B-E).[61,62] Dopamine receptor messenger RNAs (mRNAs) are very difficult to detect with conventional techniques at the single-cell level, even in striatal neurons, but this low transcript expression allows sufficient generation of functional protein.[63] Accordingly, we found that Drd2 expression in LSK cells, HSCs (Lin$^-$ Sca1$^+$ cKit$^+$ CD48$^-$ CD150$^+$), and c-Kit$^+$ Lin$^-$ hematopoietic cells is supported by analysis of *Drd2-EGFP* transgenic mice and by qPCR (Figure 1C-D; supplemental Figure 1F-G). Furthermore, immunostaining confirms expression of Drd2 and Drd3 in c-Kit$^+$ Lin$^-$ hematopoietic cells in adult BM sections and in freshly isolated LSK cells and HSCs (Figure 1E-F; supplemental Figure 1H-K). Expression of Drd2 and Drd3 in LSK cells and HSCs, but not in differentiated hematopoietic cells, is also evident by flow cytometry (Figure 1G-H; supplemental Figure 1L-M). Based on FACS analysis, the expression of Drd2 is 1.9-fold higher in neurons than in LSK cells, whereas neuronal Drd3 is 0.7-fold lower than in LSK cells (supplemental Figure 1N). Although D_1-type receptor expression is detectable in LSK cells, pharmacological inhibition with the D_1-specific inhibitor SCH-23390 does not cause hematopoietic defects (supplemental Figure 2A-B).[64]

To investigate the potential functions of D_2-type receptors in HSC maintenance, we analyzed young adult *Drd2*-knockout (*Drd2*$^{-/-}$) and *Drd3*-knockout (*Drd3*$^{-/-}$) mice. Remarkably, *Drd2*$^{-/-}$ and *Drd3*$^{-/-}$ mice exhibit a reduction in HSCs and LSK cells in BM (supplemental Figure 2C-D). We further generated *Drd2* and *Drd3* double-knockout (*Drd*-DKO) mice, which also show significant loss of HSCs and LSK cells relative to wild-type (WT) controls (Figure 1I-J). Loss of HSCs in *Drd*-DKO mice is confirmed by CD45.2/CD45.1 competitive repopulation (Figure 1K; supplemental Figure 2E-F). Similar to findings in BM, LSK cells and HSCs are also reduced in *Drd*-DKO spleen, whereas the abundance of these cell populations in peripheral blood is unaltered (supplemental Figure 2G). Although total BM nucleated cells (BMNCs) are comparable in *Drd*-DKO and control samples, mutants show a substantial reduction in common myeloid progenitors, megakaryocyte–erythroid progenitors, CD11b$^+$ myeloid cells, and Gr-1$^+$ granulocytes (supplemental Figure 2H-J). Together, these results establish that D_2-type receptors are expressed by HSCs/HSPCs and are necessary for maintenance of these cell populations.

Next, we conducted experiments to distinguish the role of D_2-type dopamine receptors in hematopoietic cells vs stromal cells. To generate hematopoietic cell–specific *Drd*-DKO chimeric mice (*Drd*-DKO$^{\Delta HC}$), lethally irradiated WT recipients were transplanted with LSK cells from WT or *Drd*-DKO donors and analyzed after successful repopulation (Figure 1L). Chimeras with *Drd*-DKO hematopoietic cells show significantly reduced percentages of HSCs and LSK cells in BM (Figure 1M; supplemental Figure 2K-L). The loss of HSCs was confirmed by secondary transplantation when transplanted recipient mice were used as donors for CD45.2/CD45.1 competitive repopulation (Figure 1N). In contrast, when lethally irradiated WT or *Drd*-DKO

Figure 1. D_2-type dopamine receptors cell-autonomously regulate HSC maintenance. (A) Normalized ratio (normalized to 1) of dopamine/noradrenaline in extracellular fluid from midbrain, BM, spleen, and thymus by ELISA (n = 4 for each tissue). The *P* values were calculated using analysis of variance (ANOVA). (B) Normalized dopamine level in extracellular fluid of midbrain, BM, spleen, and thymus by ELISA (n = 4). The *P* values were calculated using ANOVA. (C) Representative FACS graphs and quantification of GFP expression in LSK cells and HSCs from littermate control or *Drd2-EGFP* transgenic mice (n = 4). The *P* value was calculated using the Student *t* test. (D) Representative confocal images showing GFP expression in Lin$^-$ c-Kit$^+$ HSPCs in adult bone sections from *Drd2-EGFP* mice. Confocal images showing Drd2 (E) and Drd3 (F) expression in FACS-sorted HSCs (left panels) and LSK cells (right panels) from WT or *Drd*-DKO (DKO) mice. Quantification of Drd2 or Drd3 normalized mean fluorescent intensity (nMFI). Mean fluorescent intensity (MFI) for WT cells is normalized to 1. For Drd2, WT HSC = 19, DKO HSC = 39, WT LSK = 33, and DKO LSK = 33. For Drd3, WT HSC = 18, DKO HSC = 21, WT LSK = 25, and DKO LSK = 25. Representative FACS graphs showing Drd2 (G) and Drd3 (H) expression in WT and *Drd*-DKO LSK cells and HSCs. MFI is normalized to the WT sample without primary antibody (n = 3); WT = 6, *Drd*-DKO = 6. (I) Representative FACS plots of LSK cells and HSCs in *Drd*-DKO and WT control mice. Numbers in the boxed areas represent the percentage of the corresponding cell population. (J) Quantification of the percentages of LSK cells (upper panels) and HSCs (lower panels) in BM (WT = 14; *Drd*-DKO = 14). The *P* value was calculated using the Student *t* test. (K) Quantification of donor-derived (CD45.2) B lymphocytes, T lymphocytes, and myeloid cells in competitive repopulating experiments (WT = 14; *Drd*-DKO = 14). A total of 5×10^5 CD45.2 (WT or *Drd*-DKO) BM cells were mixed with 5×10^5 CD45.1 BM cells, transplanted into lethally irradiated CD45.1 recipients, and analyzed 16 weeks later. The *P* value was calculated using the Student *t* test. (L) Diagram depicting transplantation of WT or *Drd*-DKO LSK cells into lethally irradiated WT mice. (M) Percentages of LSK cells (left panel), HSCs (middle panel), and CD49b$^-$ HSCs (right panel) in hematopoietic-specific chimeric WT (n = 11) or *Drd*-DKO$^{\Delta HC}$ (n = 8) BM from mice in panel L at 6 months after transplantation. The *P* value was calculated using the Student *t* test. (N) Quantification of donor-derived (CD45.2) cells in secondary competitive transplantation experiments (WT donor BM = 9; *Drd*-DKO$^{\Delta HC}$ donor BM = 12). The *P* value was calculated using the Student *t* test. (O) Schematic diagram depicting transplantation of WT LSK cells into lethally irradiated WT or *Drd*-DKO recipients. (P) Percentages of LSK cells (left panel), HSCs (middle panel), and CD49b$^-$ HSCs (right panel) from chimeric mice in panel O at 6 months after transplantation. The *P* value was calculated using the Student *t* test. WT = 11; *Drd*-DKO$^{\Delta SC}$ = 7. APC, allophycocyanin; Ctrl, control; Fig.S2L, supplemental Figure 2L; Fig.S2M, supplemental Figure 2M; FITC, fluorescein isothiocyanate; PE, phycoerythrin.

Downloaded from http://ashpublications.net/blood/article-pdf/138/21/2051/1868550/bloodbld2020010419.pdf by guest on 29 May 2024

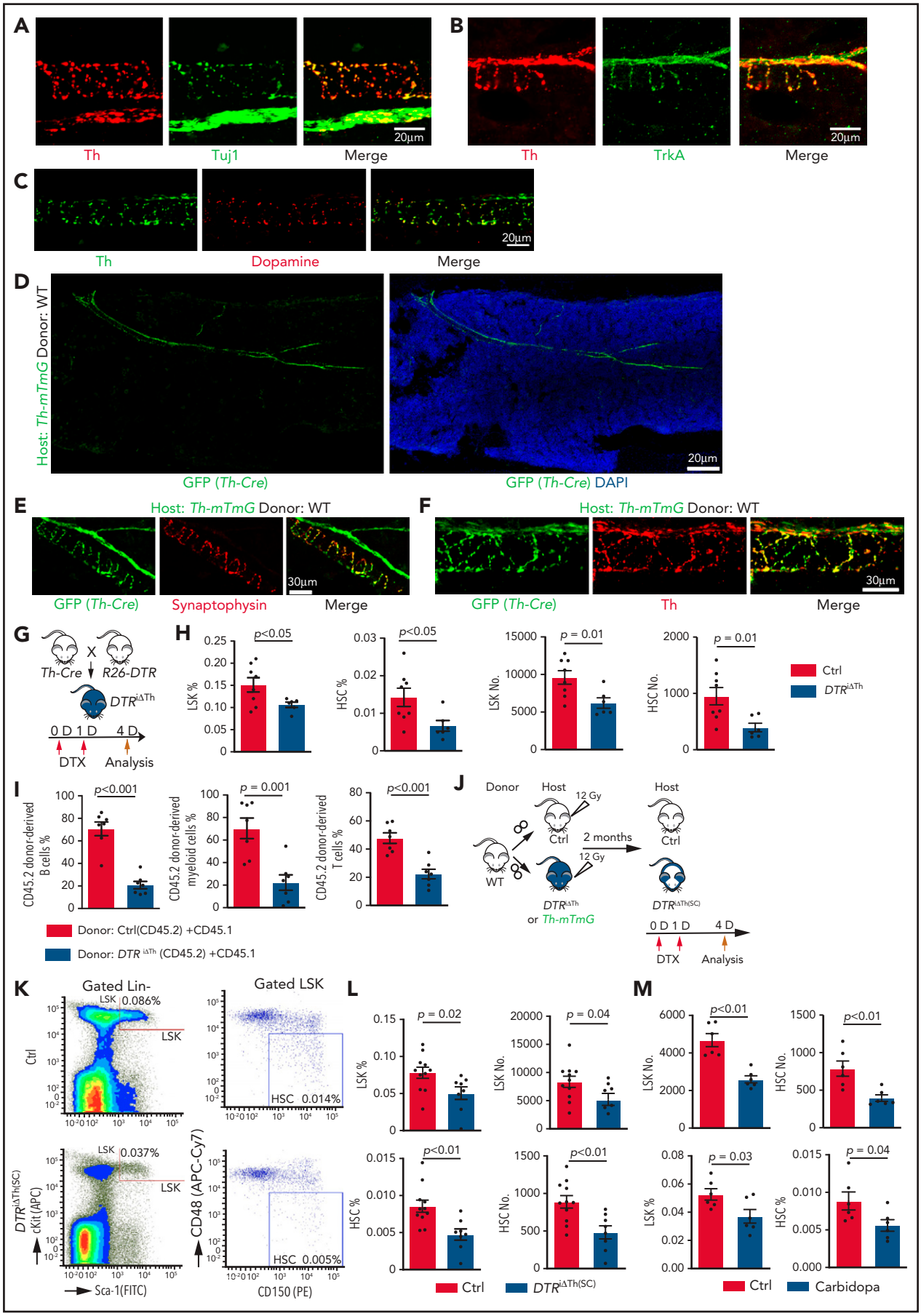

Figure 2.

Downloaded from http://ashpublications.net/blood/article-pdf/138/21/2051/1868550/bloodbld2020010419.pdf by guest on 29 May 2024

recipients were transplanted with WT donor LSK cells and analyzed after successful repopulation, HSC and LSK cell percentage were not significantly different in the resulting stromal cell–specific *Drd*-DKO (*Drd*-DKO$^{\Delta SC}$) chimeras (Figure 1O-P; supplemental Figure 2M) lacking Drd2/Drd3 in nonhematopoietic cells. The observed differences in transplantation experiments with *Drd*-DKO cells are highly unlikely to be caused by a mixed genetic background, because we obtained very similar results with WT cells from C57/B6 or 129 mice (supplemental Figure 2N-P). Moreover, acute administration of haloperidol, which has high affinity for D_2-type dopamine receptors and 50-fold to 4000-fold lower binding to other receptors, including serotonin and adrenergic receptors,[64] results in a significant reduction in the percentage of LSK cells and HSCs (supplemental Figure 2Q-S) that involves increased apoptosis of these cells but is not related to altered levels of the chemokine Cxcl12 and SCF in BM (supplemental Figure 2T-V).

These results indicate that D_2-type dopamine receptors are required for HSC and LSK cell maintenance in hematopoietic but not BM stromal cells. Furthermore, the above findings establish that alterations in *Drd*-DKO HSCs and progenitors are not caused indirectly (eg, by defects in brain physiology).

Blockade of dopamine synthesis phenocopies loss of HSCs and HSPCs

Next, we investigated whether blockade of dopamine synthesis results in a similar phenotype as does inactivation of D_2-type receptors. Because Th is essential for dopamine synthesis, the neuromodulator can only be released by Th$^+$ cell populations; accordingly, dopamine immunostaining is seen along Th$^+$ nerve fibers in BM, which are also positive for Tuj1 (neuron-specific class 3 β-tubulin) and the neurotrophin receptor TrkA (Figure 2A-C; supplemental Figure 3A-B). In contrast, Th signal is undetectable in Emcn$^+$ endothelial cells, Lepr$^+$ mesenchymal cells, αSMA$^+$ vascular smooth muscle cells, and lineage-committed hematopoietic cells (supplemental Figure 3C-F). This expression pattern is confirmed by a genetic approach involving a combination (*Th-mTmG*) of constitutively active *Th-Cre* and *Rosa26-mTmG* Cre reporter mice (supplemental Table 1). In lethally irradiated *Th-mTmG* mice transplanted with WT donor BM cells (Figure 2D), the GFP signal colocalizes with the presynaptic marker synaptophysin and endogenous Th (Figure 2E-F; supplemental Figure 3G-J). Furthermore, immunostaining shows that CD150$^+$ CD48$^-$ CD41$^-$ Lin$^-$ HSCs are enriched in the vicinity of GFP$^+$ nerves relative to random cells in *Th-mTmG* recipient mice (supplemental Figure 3K-L).

To block dopamine synthesis in nerves, we generated *Th-Cre Rosa26-DTR* (*DTR*$^{i\Delta Th}$) mice in which diphtheria toxin (DTX) administration ablates Th$^+$ cells (Figure 2G). This strategy efficiently eliminates Th$^+$ signals, which are readily detectable around αSMA$^+$ vascular smooth muscle cell–covered arteries in control, but not in *DTR*$^{i\Delta Th}$, BM (supplemental Figure 3M) and causes a significant reduction in dopamine levels in *DTR*$^{i\Delta Th}$ BM extracellular fluid (supplemental Figure 3N-Q). DTX administration to Cre$^-$ mice does not influence the percentage of LSK cells, indicating that DTX does not influence HSPCs in an unspecific fashion (supplemental 3R). In contrast, nerve ablation in Cre$^+$ *DTR*$^{i\Delta Th}$ mice leads to a significant decrease in LSK cells and HSCs, as well as reduced proliferation in young adults (Figure 2H; supplemental Figure 3S). The reduction in HSCs is confirmed by CD45.2/CD45.1 competitive repopulation assay (Figure 2I).

To confirm that defects in *DTR*$^{i\Delta Th}$ mice are indeed induced by ablation of stromal Th$^+$ cells, we transplanted lethally irradiated *DTR*$^{i\Delta Th}$ and control mice with WT BM cells and administered DTX after successful reconstitution [*DTR*$^{i\Delta Th(SC)}$] (Figure 2J). In the presence of WT hematopoietic cells, *DTR*$^{i\Delta Th(SC)}$ recipients show a significant reduction in LSK cells and HSCs after DTX administration (Figure 2K-L).

Next, we interfered with dopamine synthesis outside of the brain by injecting carbidopa, which cannot cross the blood-brain barrier and, therefore, prevents conversion of L-3, 4-dihydroxyphenylalanine to dopamine by inhibiting the enzyme aromatic L-amino acid decarboxylase only in the peripheral nervous system.[65] Consistent with our other findings, carbidopa treatment results in a significant reduction in LSK cells and HSCs (Figure 2M). Because Th is also required for the synthesis of noradrenaline and adrenaline, we administered the inhibitor ICI-118551 intraperitoneally to block the β_2 adrenergic receptor,[42] which does not induce significant changes in LSK cell percentage and hematopoiesis (supplemental Figure 4A-D). Together with 2 recent reports showing that young adult knockout mice lacking the β_3 adrenergic receptor or the β_2 and β_3 adrenergic receptors do not exhibit a significant reduction in LSK cells,[42,44] these findings argue that defective noradrenaline/adrenaline function is unlikely to be a major cause of the defective HSPC maintenance in young adult *DTR*$^{i\Delta Th(SC)}$ mice.

Thus, depletion of dopamine results in loss of HSCs and HSPCs, which phenocopies defects in *Drd*-DKO mice, arguing for direct regulation by dopamine.

Figure 2. Blockade of dopamine synthesis impairs HSC maintenance. Representative confocal images showing expression pattern of endogenous Th protein in combination with Tuj1 (A) and TrkA (B) in WT BM. (C) Immunostaining showing distribution of dopamine and its colocalization with Th in BM. (D) Tile-scan image showing *Th-Cre*–driven GFP expression in *Th-mTmG* recipient BM. Colocalization of *Th-Cre*–driven GFP with neuronal presynaptic marker synaptophysin (E) and Th protein (F) in *Th-mTmG* recipients. (G) Diagram depicting genetic strategy for Th$^+$ cell ablation after DTX administration. (H) Quantification of the percentages and numbers of LSK cells and HSCs in BM of *DTR*$^{i\Delta Th}$ (Cre$^{+/T}$ flox$^{+/f}$; n = 6) and control (Cre$^{+/+}$ flox$^{+/f}$; n = 8) mice. The *P* value was calculated using the Student *t* test. (I) Quantification of donor-derived (CD45.2) B lymphocytes, T lymphocytes, and myeloid cells in competitive repopulating assay. A total of 5×10^5 CD45.2 (Ctrl or *DTR*$^{i\Delta Th}$) BM cells mixed with 5×10^5 CD45.1 BM cells were transplanted into lethally irradiated CD45.1 recipients, which were analyzed 16 weeks later. Ctrl = 7; *DTR*$^{i\Delta Th}$ = 7. The *P* value was calculated using the Student *t* test. (J) Schematic diagram depicting WT BM transplantation into *DTR*$^{i\Delta Th}$ and control mice. DTX injection and HSC analysis were done 2 months after transplantation. *Th-mTmG* reporter mice were analyzed without toxin injection. (K) Representative FACS plots of LSK cells and HSCs in control and *DTR*$^{i\Delta Th(SC)}$ recipients after DTX administration. Numbers represent the percentages of the indicated cell populations in BM. (L) Quantification of the percentages (left panels) and numbers (right panels) of LSK cells and HSCs in control (n = 11) and *DTR*$^{i\Delta Th(SC)}$ (n = 8) recipient BM. The *P* value was calculated using the Student *t* test. (M) Quantification of the numbers and percentages of LSK cells and HSCs in BM from vehicle-injected (n = 6) or carbidopa-injected (n = 6) WT mice. The *P* value was calculated using the Student *t* test. APC, allophycocyanin; Ctrl, control; FITC, fluorescein isothiocyanate; PE, phycoerythrin.

Downloaded from http://ashpublications.net/blood/article-pdf/138/21/2051/1868550/bloodbld2020010419.pdf by guest on 29 May 2024

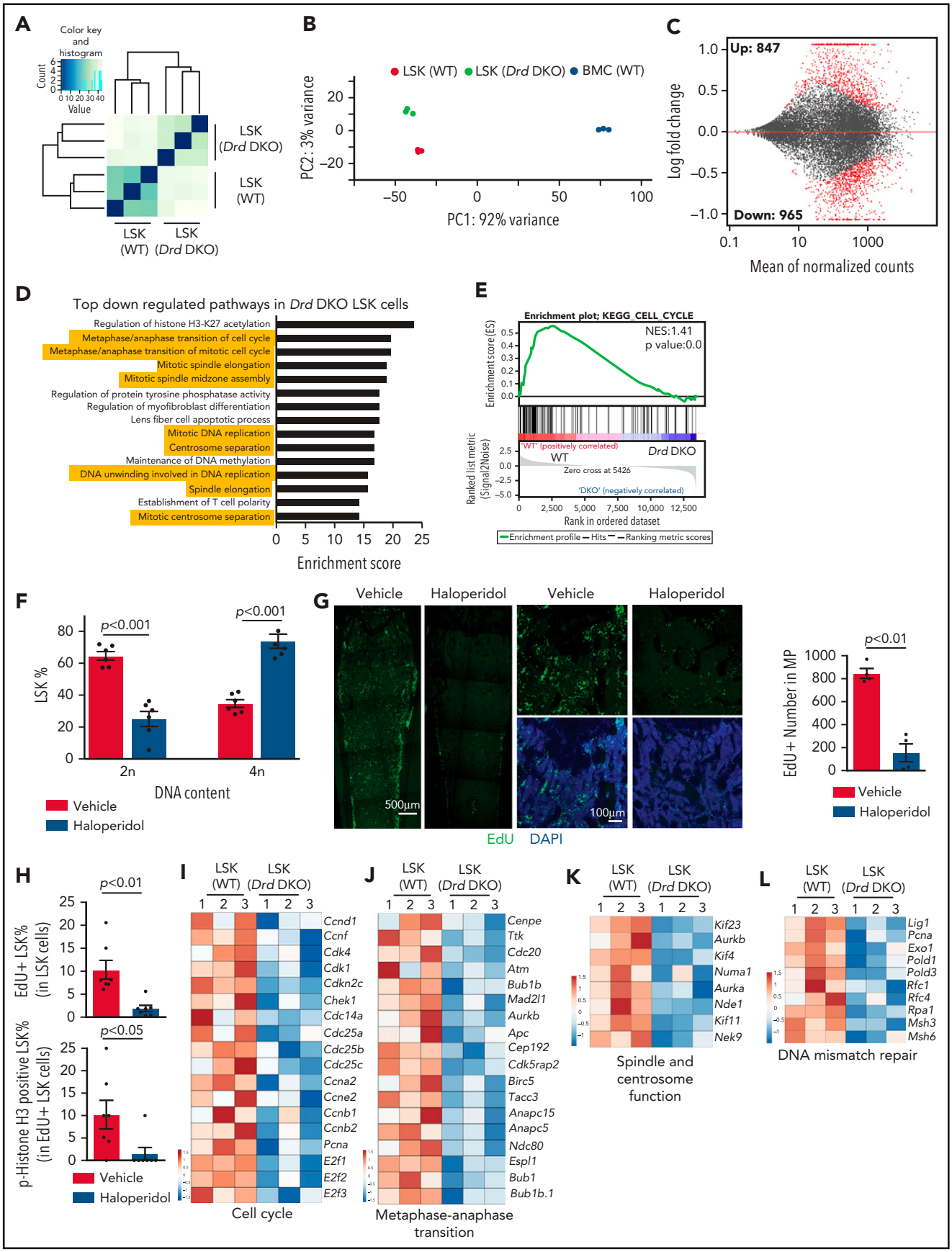

Figure 3.

Downloaded from http://ashpublications.net/blood/article-pdf/138/21/2051/1868550/bloodbld2020010419.pdf by guest on 29 May 2024

Loss of dopamine signaling alters the transcription profile and cell cycle status of LSK cells

To address how dopamine regulates the functional properties of LSK cells, we sorted this population from WT and *Drd*-DKO mice for bulk RNA-seq analysis. Unsupervised clustering and principal component analysis of the RNA-seq data show that *Drd*-DKO LSK cell replicates are more similar to each other than to WT LSK cells (Figure 3A-B; supplemental Figure 4E). In a Bland-Altman plot, knockout of *Drd2* and *Drd3* results in the upregulation of 847 genes and downregulation of 965 genes at a significance of $P < .05$ (Figure 3C), which further supports a cell-autonomous function for dopamine signaling in LSK cells. Based on gene ontology analysis, several pathways controlling cell cycle and mitosis are among the top regulated candidates (Figure 3D). Downregulation of cell cycle–related genes and pathways are detected by Kyoto Encyclopedia of Genes and Genomes (KEGG) analysis (Figure 3E), which also reveals changes in other signaling activities (supplemental Figure 4F-G). Similar to *Drd*-DKO LSK cells, haloperidol treatment results in significant transcriptional changes and cell cycle defects in LSK cells (supplemental Figure 4H-L). These results indicate that D_2-type receptors maintain the transcriptional profile and cell cycle status of LSK cells.

Next, we used several approaches to block dopamine signaling and study the effects on LSK cell mitosis. After haloperidol treatment, DNA content analysis shows significant enrichment of LSK cells in the tetraploid state (Figure 3F), which may reflect active proliferation or, alternatively, cell cycle arrest at the G_2/M checkpoint. Arguing for the latter, transient (1-hour) EdU (5-ethynyl-2'-deoxyuridine) incorporation in vivo is significantly reduced in haloperidol-treated BM samples (Figure 3G). Haloperidol also reduces LSK cell proliferation, as indicated by the significant reduction in EdU incorporation and phospho-histone $H3^+$ EdU^+ double-positive LSK cells (Figure 3H). This is consistent with RNA-seq data showing downregulation of genes related to cell cycle, metaphase-anaphase transition, spindle/centrosome function, and DNA-mismatch repair in *Drd*-DKO LSK cells (Figure 3I-L). Furthermore, we detect accumulation of γH2Ax, a DNA damage marker, after haloperidol treatment (supplemental Figure 4M-N).[66] These results establish that D_2-type receptor activity preserves gene expression related to the proliferation and cell cycle status of LSK cells under steady-state conditions.

D_2-type dopamine receptors regulate BM transplantation efficiency

Next, we investigated whether D_2-type receptors play a role in allogeneic BM transplantation after lethal irradiation.[32,67] We analyzed the transplantation efficiency at 2 weeks after transplantation, which is within the critical period for recipient survival that requires rapid proliferation and expansion of transplanted HSPCs.[13,22,68] Irradiated WT recipients that had received *Drd*-DKO LSK cells (*Drd*-DKO$^{\Delta HC}$) show significantly delayed hematopoietic reconstitution, with lower numbers of BMNCs, LSK cells, and $CD45^+$ leukocytes relative to controls receiving WT LSK cells (Figure 4A-C). *Drd*-DKO LSK transplant-derived cells show a reduced Ki67 signal in BM, indicating reduced proliferation (Figure 4D). In contrast, no significant differences in hematopoietic reconstitution are detected 2 weeks after transplantation of WT LSK cells into lethally irradiated WT or *Drd*-DKO recipients (Figure 4E-G). Thus, D_2-type dopamine receptors in hematopoietic cells, but not in stromal cells, are critical for BM transplantation.

We also transplanted Lin^- cells ($Ter119^-$ $CD5^-$ $CD11b^-$ $CD45R^-$ Ly-6G/C^-) from *Vav1-Cre Rosa26-mTmG* double-transgenic mice, in which Lin^- cells and their descendants are genetically labeled by GFP expression (Figure 4H; supplemental Figure 5A). Transplantation of these cells into *DTR*$^{i\Delta Th}$ mice or haloperidol-treated WT recipients results in substantially lower transplantation efficiency, as indicated by the percentage of GFP^+ cells in recipients (Figure 4I-K; supplemental Figure 5B-D). EdU incorporation and the percentage of EdU^+ cells in the GFP^+ (donor-derived) population are significantly lower in *DTR*$^{i\Delta Th}$ mice and in haloperidol-treated mice, which are indicative of proliferation defects (Figure 4I-K; supplemental Figure 5B-E). These data establish that genetic or pharmacological blockade of dopamine signaling results in lower transplantation efficiency.

Next, we investigated the effect of irradiation on dopamine synthesis. At 7 days after lethal irradiation without transplantation, the total density of nerve fibers in BM is not changed (supplemental Figure 6A-B). In contrast, Th^+ puncta number per length of nerve, as well as the signals for the presynaptic marker synaptophysin$^+$, is reduced (Figure 5A-B; supplemental Figure 6C), which is accompanied by lower levels of dopamine in femoral extracellular fluid and bone sections (Figure 5C; supplemental Figure 6D-E). Because these alterations are indicative of functional defects in bone nerves and reduced dopamine production in BM after irradiation, we tested whether activation of D_2-type receptors with the agonist 7-OH-DPAT can improve the transplantation process. Lin^- donor cells from *Vav1-Cre R26-mTmG* mice were transplanted into lethally irradiated recipients in combination with repeated 7-OH-DPAT or vehicle administration once daily for 5 days (Figure 5D). 7-OH-DPAT treatment after transplantation leads to a significant increase in the percentage of GFP^+ cells in recipient BM and a higher percentage of donor-derived leukocytes (Figure 5E-H). EdU incorporation into donor-derived (GFP^+) cells is also increased, indicating that 7-OH-DPAT treatment promotes their expansion after transplantation (Figure 5F-H). Prolonged 7-OH-DPAT treatment every second day for 12 days (Figure 5I) increases LSK cell percentage, the number of BMNCs and $CD45^+$ leukocytes in BM, indicating

Figure 3. D_2-type dopamine receptors regulate the transcription profile and cell cycle status of LSK cells. Unsupervised clustering (A) and principal components analysis (B) of RNA-seq results from *Drd-DKO* and WT LSK cells. (C) Bland-Altman plot showing 847 upregulated and 965 downregulated genes in *Drd-DKO* LSK cells relative to control at $P < 0.05$ significance level. Red dots indicate differentially expressed genes. (D) Gene ontology analysis indicating the top downregulated pathways in *Drd-DKO* LSK cells. The yellow highlighting denotes cell cycle and mitosis-related pathways. (E) KEGG analysis indicating downregulation of the cell cycle pathway in *Drd-DKO* LSK cells. (F) Percentage of LSK cells with diploid (2n) or tetraploid (4n) DNA content after treatment with vehicle (n = 6) or haloperidol (n = 6). The *P* value was calculated using the Student *t* test. (G) Maximum intensity projections showing EdU incorporation in sections of distal long bone and, at higher magnification, in metaphysis after haloperidol treatment (left panels). Quantification of the number of EdU^+ cells in metaphysis (area = 1 mm^2) (right panel). Vehicle = 4; haloperidol = 4. (H) FACS-based quantification of EdU^+ LSK cells and p-Histone $H3^+$ EdU^+ LSK cells after haloperidol treatment. The *P* value was calculated using the Student *t* test. Vehicle = 7; haloperidol = 7. Heat map of selected cell cycle (I), metaphase-anaphase transition (J), spindle/centrosome function (K), and DNA mismatch repair–related genes (L) in *Drd-DKO* and WT LSK cells.

Downloaded from http://ashpublications.net/blood/article-pdf/138/21/2051/1868550/bloodbld2020010419.pdf by guest on 29 May 2024

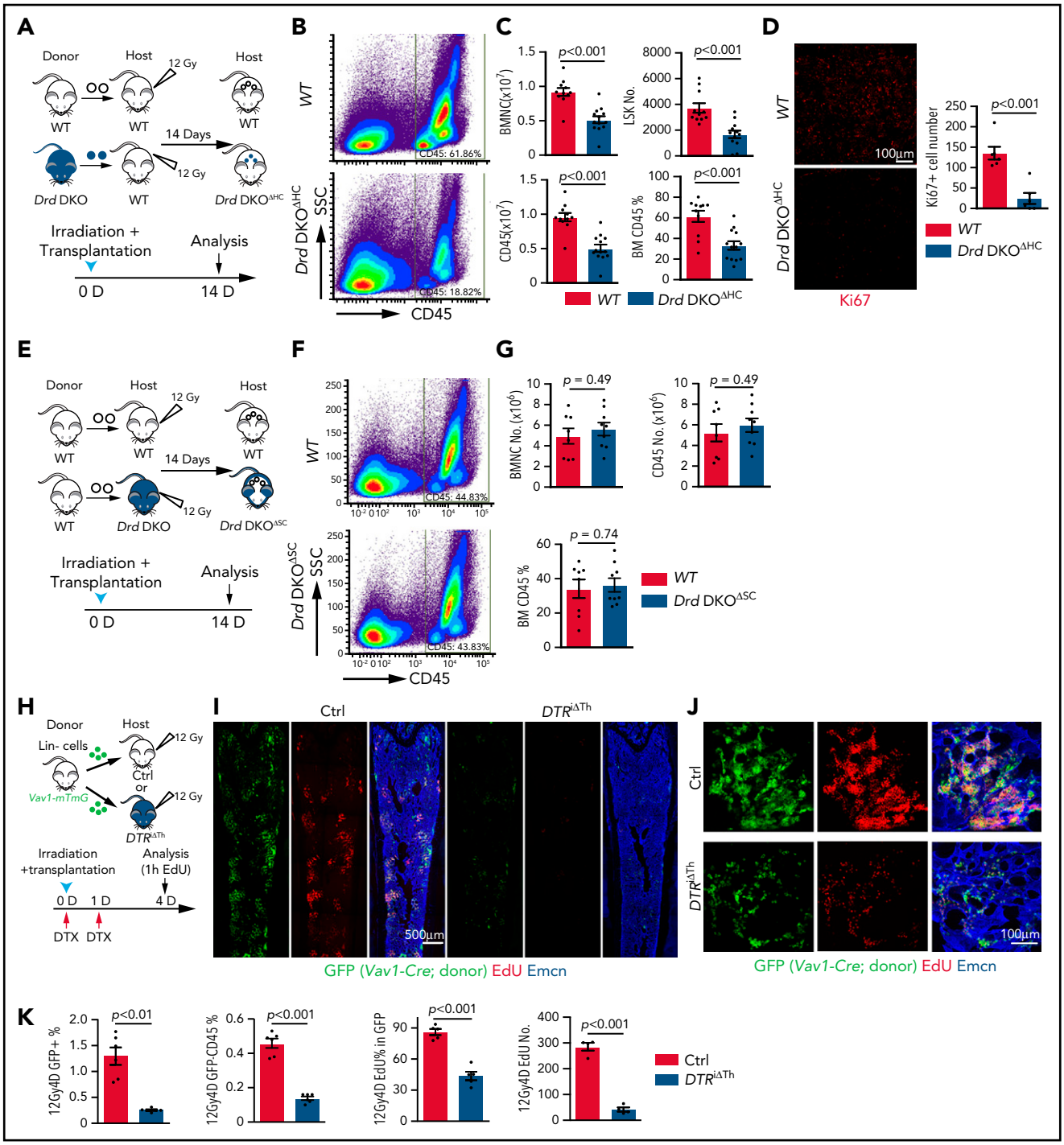

Figure 4. D_2-type dopamine receptors regulate BM transplantation efficiency. (A) Diagram depicting the transplantation of WT or *Drd*-DKO LSK cells into lethally irradiated WT mice. (B) Pseudocolor FACS plot of $CD45^+$ leukocytes in recipient BM, analyzed 14 days after transplantation. Numbers in rectangles represent the percentages of gated cells. (C) Quantification of BMNCs, LSK cells, and $CD45^+$ cells (WT = 11; *Drd*-$DKO^{\Delta HC}$ = 13). The *P* value was calculated using the Student *t* test. (D) Confocal image of Ki67 staining in bone sections from recipients transplanted with WT or *Drd*-DKO cells (left panels). Quantification of $Ki67^+$ cell number in each image field (right panel; WT = 6; *Drd*-$DKO^{\Delta HC}$ = 6). The *P* value was calculated using the Student *t* test. (E) Diagram depicting transplantation of LSK cells from WT mice into lethally irradiated WT or *Drd*-DKO recipients. (F) Representative FACS plot of $CD45^+$ leukocytes in WT or *Drd*-$DKO^{\Delta SC}$. Numbers in boxed areas represent the percentage of cells in the BM. (G) Quantification of BMNC and $CD45^+$ cell number in WT (n = 8) or *Drd*-$DKO^{\Delta SC}$ (n = 9) recipients. The *P* value was calculated using the Student *t* test. (H) Scheme illustrating the lethal irradiation (12 Gy) of $DTR^{i\Delta Th}$ and littermate controls and transplantation of genetically labeled (GFP^+) Lin^- HSPCs from *Vav1-Cre Rosa26-mTmG* donors (day 0) and treatment with DTX on days 0 and 1. Following EdU injection at day 4, mice were euthanized 1 hour later for immunostaining and FACS analysis. (I) Overview of bone sections from $DTR^{i\Delta Th}$ or littermate control mice after lethal irradiation and transplantation of GFP-labeled donor cells. Green, donor-derived hematopoietic cells; red, EdU; blue, Emcn. (J) Representative confocal images of bone sections showing GFP^+ cells (green), $Emcn^+$ endothelial cells (blue), and EdU incorporation (red) in $DTR^{i\Delta Th}$ (lower panels) or littermate control (upper panels) mice. (K) Percentage of donor-derived GFP^+ and GFP^+ $CD45^+$ cells by FACS (Ctrl = 6; $DTR^{i\Delta Th}$ = 6). Quantification of EdU^+ cells in each field by imaging (Ctrl = 5; $DTR^{i\Delta Th}$ = 5). The *P* value was calculated using the Student *t* test. 1h, 1 hour; 12Gy4D, 4 days after lethal irradiation at 12Gy; Ctrl, control; D, day; SSC, side scatter.

Downloaded from http://ashpublications.net/blood/article-pdf/138/21/2051/1868550/bloodbld2020010419.pdf by guest on 29 May 2024

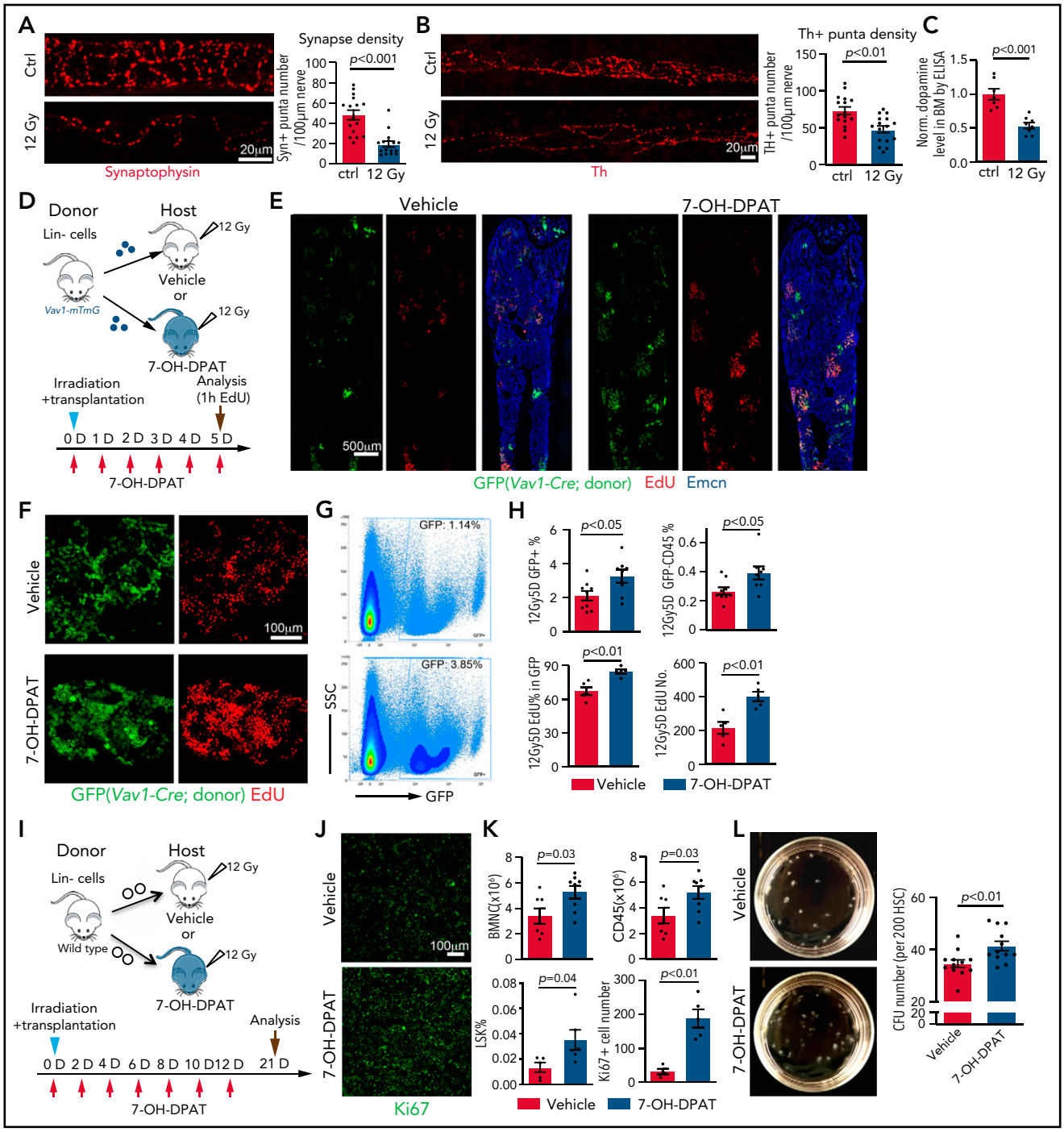

Figure 5. The D_2-type receptor agonist 7-OH-DPAT promotes BM transplantation efficiency. Representative confocal images showing synaptophysin (A) and Th. The *P* value was calculated using the Student *t* test. (B) immunosignal in control (Ctrl) and irradiated BM at 7 days after 12 Gy irradiation. Quantification of the synaptophysin$^+$ and Th$^+$ puncta per length nerve. Ctrl = 16 slices from 3 mice; 12 Gy = 16 slices from 3 mice. (C) ELISA of dopamine levels in flushed BM extracellular fluid in control (ctrl) femur (n = 7) or 7 days after lethal irradiation (12 Gy) (n = 8). The *P* value was calculated using the Student *t* test. (D) Transplantation of Lin$^-$ cells from *Vav1-Cre Rosa26-mTmG* mice into 7-OH-DPAT–treated (short regimen, as indicated) or vehicle control mice after lethal irradiation. (E) Overview of bone sections from 7-OH-DPAT–treated or control mice after lethal irradiation and transplantation of GFP-labeled donor cells. (F) Representative confocal images showing GFP$^+$ donor cells (green) and EdU incorporation (red) in sections from vehicle- and 7-OH-DPAT–treated long bone at 5 days after lethal irradiation and transplantation. (G) Representative FACS plot of GFP$^+$ cells in irradiated and transplanted mice treated with vehicle or 7-OH-DPAT. (H) Quantification of the percentages of GFP$^+$ cells and donor-derived CD45$^+$ cells in BM by FACS (vehicle = 9; 7-OH-DPAT = 8). Quantification of EdU$^+$ cells by imaging (vehicle = 5; 7-OH-DPAT = 5). The *P* value was calculated using the Student *t* test. (I) Schematic depiction of the transplantation of Lin$^-$ cells into 7-OH-DPAT–treated or vehicle control recipients (long treatment regimen) at day 21 after lethal irradiation. (J) Confocal images showing Ki67$^+$ signal in bone sections from recipients treated with vehicle or 7-OH-DPAT. (K) Quantification of the numbers of BMNCs and CD45$^+$ cells and the percentages of LSK cells (vehicle = 7; 7-OH-DPAT = 8). The *P* value was calculated using the Student *t* test. Quantification of Ki67$^+$ cell number in each image field in panel J (vehicle = 4; 7-OH-DPAT = 5). (L) Representative images (dish at day 8 after seeding) (left panels) and quantification of CFU from 200 HSCs isolated from WT mice (right panel). 7-OH-DPAT or vehicle was added to MethoCult medium (vehicle = 12; 7-OH-DPAT = 12). The *P* value was calculated using the Student *t* test. 1h, 1 hour; D, day; SSC, scatter.

Downloaded from http://ashpublications.net/blood/article-pdf/138/21/2051/1868550/bloodbld2020010419.pdf by guest on 29 May 2024

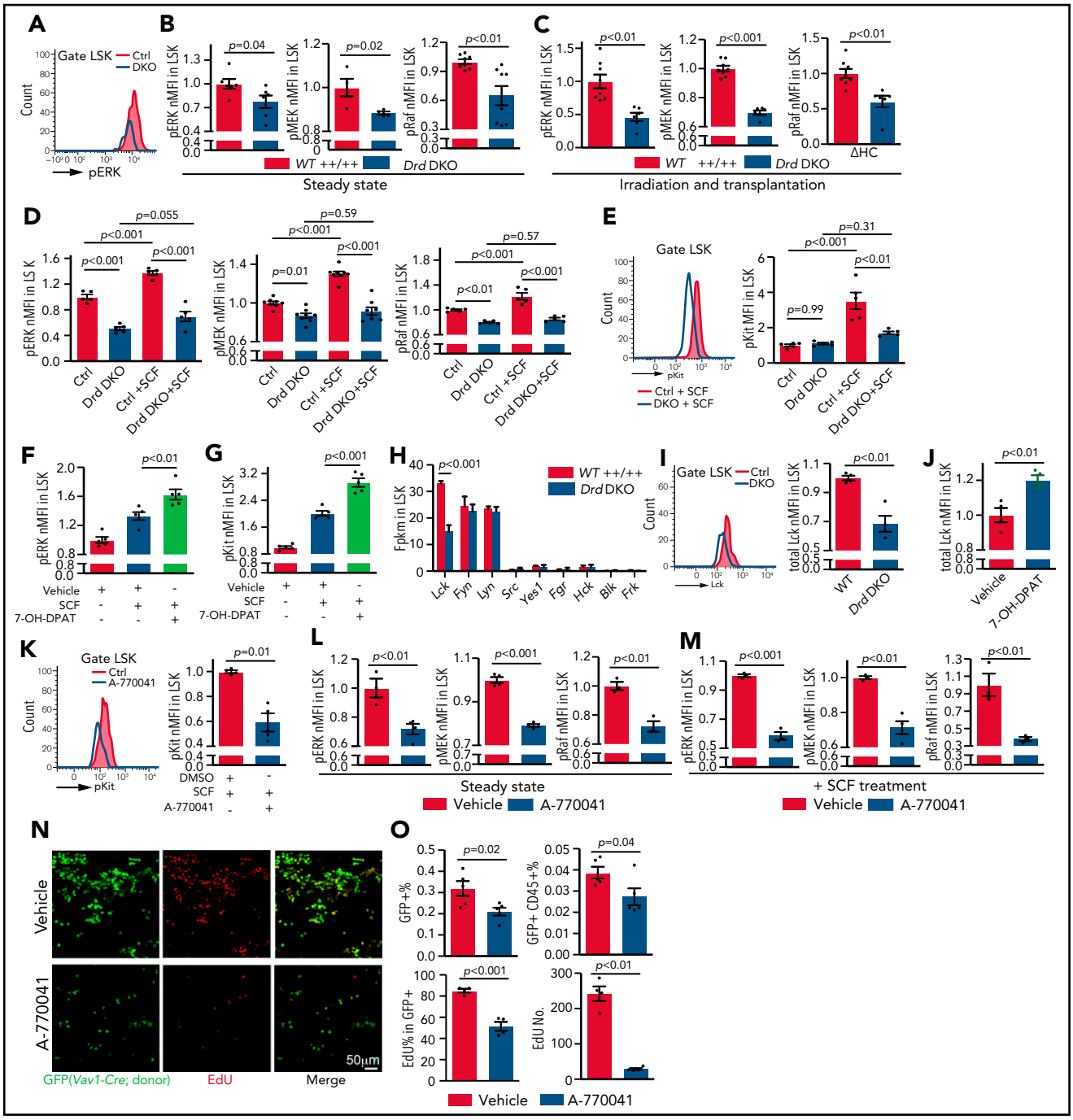

Figure 6. Dopamine regulates SCF/ERK signaling and Lck expression. (A) Representative line graph showing pERK in unstimulated *Drd*-DKO and control (Ctrl) LSK cells. (B) Normalized mean fluorescent intensity (nMFI) of ERK pathway protein phosphorylation in steady-state WT (n = 4-8) or *Drd*-DKO (n = 4-8) LSK cells. The *P* value was calculated using the Student *t* test. (C) ERK pathway phosphorylation in LSK cells from lethally irradiated mice at 14 days after transplantation with WT (n = 8) or *Drd*-DKO (n = 6) donor LSK cells. The *P* value was calculated using the Student *t* test. (D) ERK pathway phosphorylation in WT (n = 5-8) or *Drd*-DKO (n = 5-8) LSK cells with or without SCF treatment. The *P* values were calculated using analysis of variance (ANOVA). (E) Representative FACS line graphs showing flow cytometric analysis of c-Kit phosphorylation in *Drd*-DKO LSK cells and their controls. Normalized MFI of pKit in WT (n = 5) and *Drd*-DKO (n = 5) LSK cells with or without SCF treatment. The *P* values were calculated using ANOVA. nMFI of pERK (F) and pKit (G) in vehicle-treated (n = 5), SCF-stimulated vehicle-treated (n = 5), or SCF-stimulated 7-OH-DPAT–treated (n = 5) LSK cells. (H) Fragments per kilobase of transcript per million mapped reads (Fpkm) for transcripts encoding SFKs in WT and *Drd*-DKO LSK cells (n = 3 each). The *P* value was calculated using the Student *t* test. (I) Representative flow cytometric line graph of Lck protein in WT and *Drd*-DKO LSK cells (left panel). nMFI of total Lck under steady-state in WT (n = 4) and *Drd*-DKO (n = 4) LSK cells (right panel). (J) nMFI of total Lck in vehicle control–treated (n = 4) or 7-OH-DPAT–treated (n = 4) LSK cells. (K) Representative FACS line graph showing flow cytometric analysis of c-Kit phosphorylation in Lck inhibitor A-770041–treated LSK cells and their controls (left panel). nMFI of pKit in SCF-stimulated vehicle-treated (n = 4) or SCF-stimulated A-770041–treated (n = 4) LSK cells (right panel). ERK pathway protein phosphorylation in vehicle control (n = 3-4) or Lck inhibitor A-770041 (n = 3-4) treated LSK cells (L) and after SCF stimulation together with vehicle (n = 3-4) or A-770041 (n = 3-4) (M) The *P* value was calculated using the Student *t* test. (N) GFP^+ cells (green) from *Vav1-Cre Rosa26-mTmG* donors and EdU incorporation (red) in sections from vehicle- or A-770041–treated long bone at 3 days after lethal irradiation and transplantation with Lin^- cells. (O) Flow cytometric quantification of GFP^+ cells and donor-derived $CD45^+$ cells in BM (vehicle = 4; A-770041 = 4; upper panels). Quantification of the number and percentages of EdU^+ cells in GFP^+ donor cells by imaging (vehicle = 4; A-770041 = 4; lower panels). The *P* value was calculated using the Student *t* test.

Downloaded from http://ashpublications.net/blood/article-pdf/138/21/2051/1868550/bloodbld2020010419.pdf by guest on 29 May 2024

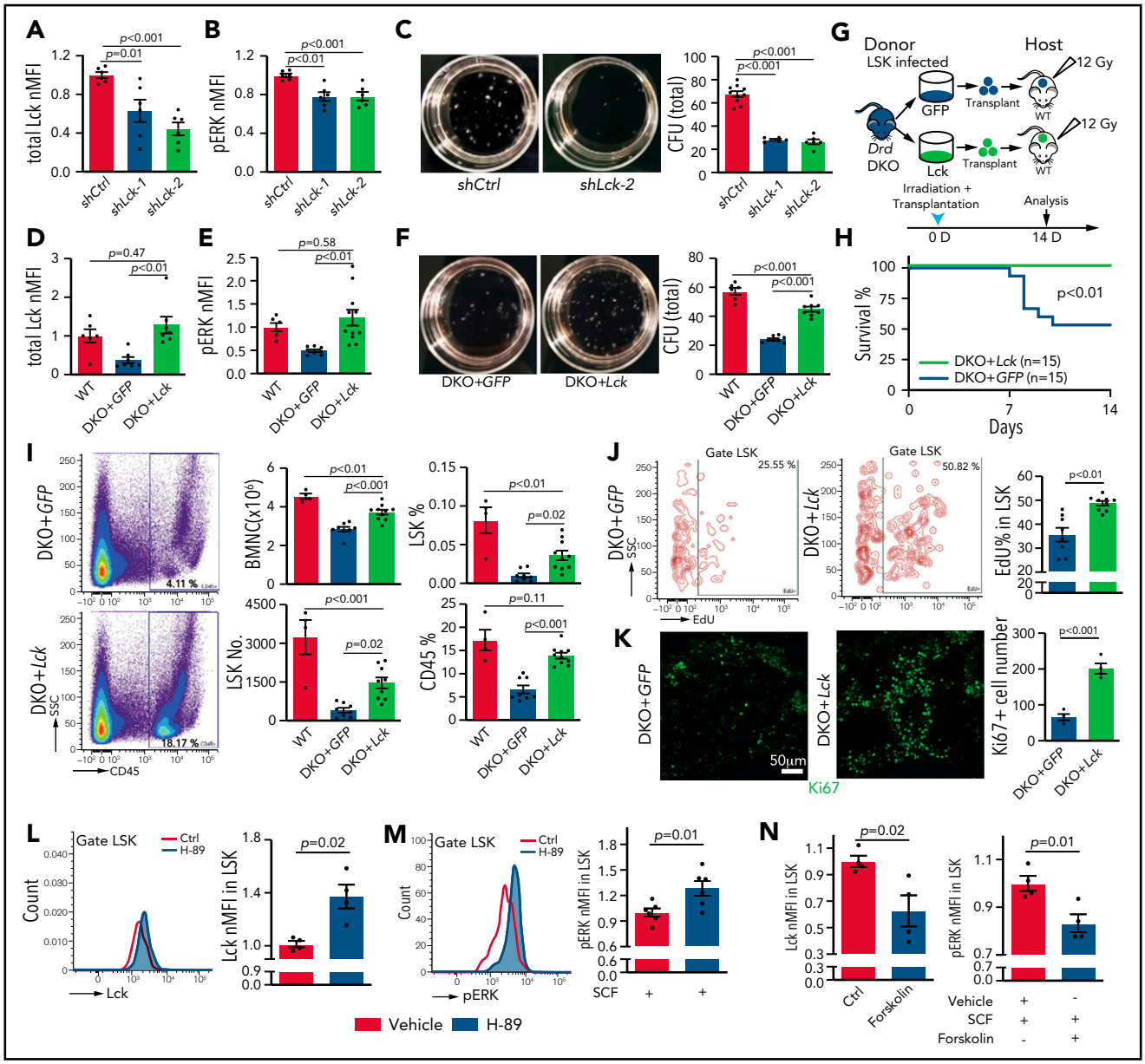

Figure 7. Lck overexpression rescues *Drd*-DKO HSPC defects. Lck protein expression (A) and pERK (B) in LSK cells infected with *shCtrl* (control *shRNA*) or *shLck* (n = 6 per group). (C) Representative images and quantification of total CFU from LSK cells infected with *shCtrl* (n = 10), *shLck-1* (n = 5), or *shLck-2* (n = 6). Lck protein expression (D) and pERK (E) in *Drd*-DKO LSK cells infected with *GFP* or *Lck* virus normalized to uninfected WT LSK cells. Total Lck, n = 6-7; pERK, n = 6-10. (F) Representative images and quantification of total CFU from *Drd*-DKO LSK cells infected with *GFP* (n = 8) or *Lck* virus (n = 8) relative to uninfected WT LSK cells (n = 6). (G) Scheme of *Drd*-DKO LSK cell infection and transplantation into lethally irradiated WT mice. (H) Survival curves after transplantation with *Drd*-DKO LSK cells infected with *GFP* (n = 15) or *Lck* virus (n = 15). Log-rank (Mantel-Cox) test was used to calculate the *P* value. (I) Representative pseudocolor plot of the percentage of $CD45^+$ cells in BM from lethally irradiated mice transplanted with DKO+*GFP* or DKO+*Lck* LSK cells (left panels). Quantitation of the numbers of BMNCs and LSK cells and the percentages of LSK cells and $CD45^+$ cells in recipients at 14 days after irradiation and transplantation (right panels). WT = 4 mice; *GFP* = 8 mice; *Lck* =10 mice. (J) Representative plots (left and middle panels) and quantitation of the percentage (right panel) of EdU^+ cells in LSK cells from mice transplanted with DKO+*GFP* or DKO+*Lck* LSK cells. *GFP* = 8 mice; *Lck* = 10 mice. The *P* value was calculated using the Student *t* test. (K) Ki67 staining in bone sections (left and middle panels) and quantitation of $Ki67^+$ cells per image field (*GFP* = 4; *Lck* = 4; right panel) from recipients transplanted with DKO+*GFP* or DKO+*Lck* LSK cells. The *P* value was calculated using the Student *t* test. (L) Representative line graph (left panel) and quantification of normalized mean fluorescent intensity (nMFI; right panel) of total Lck after H-89 treatment ex vivo (Ctrl = 4; H-89 = 4). (M) Representative line graph (left panel) and quantification of nMFI (right panel) of pERK after H-89 treatment together with SCF ex vivo (Ctrl = 6; H-89 = 6). (N) Quantification of nMFI of total Lck (left panel) and of pERK (right) after forskolin treatment together with SCF ex vivo (Ctrl = 4; forskolin = 4). In (A-F,I), the *P* values were calculated using analysis of variance. Ctrl, control; SSC, side scatter.

better recovery after transplantation (Figure 5J-K). These effects are accompanied by an increase in Ki67 signal, indicating more active proliferation in BM (Figure 5J-K). 7-OH-DPAT also significantly increases the number of colony-forming units (CFU) from FACS-sorted HSCs seeded in methylcellulose (Figure 5L; supplemental Figure 6F). These in vitro results strongly support a cell-autonomous function for D_2-type receptors in HSCs.

When Lin^- donor cells from *Drd*-DKO mice are transplanted together with 7-OH-DPAT treatment, the beneficial effect of

Downloaded from http://ashpublications.net/blood/article-pdf/138/21/2051/1868550/bloodbld2020010419.pdf by guest on 29 May 2024

7-OH-DPAT during transplantation is abolished (supplemental Figure 6G), confirming that the major target of 7-OH-DPAT to promote transplantation is through its interaction with D_2-type dopamine receptors. Treatment of sorted LSK cells from WT mice, but not from *Drd*-DKO mice, with 7-OH-DPAT in vitro results in a significant increase in HSC number (supplemental Figure 6H-I). Transplantation of 7-OH-DPAT–treated WT LSK donor cells leads to higher repopulation efficiency relative to vehicle control (supplemental Figure 6J-K). These results indicate that the activation of D_2-type dopamine receptors on HSCs and LSK cells can promote hematopoietic reconstitution after irradiation and transplantation.

Dopamine regulates Lck expression to influence ERK/MAPK signaling in LSK cells

Next, we investigated how dopamine exerts its effect on signaling in LSK cells under steady-state conditions and after BM transplantation. It is well established that extracellular regulated protein kinase (ERK)/MAPK signaling controls cell cycle and survival.[69,70] Loss of ERK has been reported to result in HSC maintenance defects.[71]

To test whether the ERK/MAPK pathway acts downstream of dopamine signaling in HSPCs, we performed intracellular immunostaining of LSK cells ex vivo using flow cytometry (supplemental Figure 7A-C).[72] At steady-state, *Drd*-DKO LSK cells exhibit lower levels of ERK/MAPK signaling, including phosphorylated ERK (pERK), pMEK, and pRaf (Figure 6A-B), whereas total ERK, MEK, and Raf are not significantly changed (supplemental Figure 7D). At 2 weeks after transplantation into lethally irradiated WT recipients, *Drd*-DKO donor–derived LSK cells show a significant reduction in the phosphorylation of the same ERK/MAPK pathway proteins (Figure 6C). Similar defects are detected in haloperidol-treated LSK cells (supplemental Figure 7E-F). This indicates that ERK pathway activity in LSK cells is controlled, in part, by dopamine signaling, which is also consistent with the known function of ERK signaling in the regulation of cell cycle and survival.[69,71]

Dopamine receptors are G protein–coupled receptors and, therefore, are unlikely to directly activate ERK signaling,[50] whereas the receptor tyrosine kinase c-Kit, the receptor for SCF, is known to trigger ERK activation.[73,74] SCF derived from endothelial and perivascular reticular niche cells plays critical roles in HSC maintenance and BM transplantation.[13,20,22] Following exposure to SCF ex vivo, *Drd*-DKO or haloperidol-treated WT LSK cells show significantly reduced phosphorylation of ERK, MEK, and Raf relative to control samples (Figure 6D; supplemental Figure 7G). SCF treatment induces phosphorylation of c-Kit at Tyr-703, a site that is required for association with Grb2 and, thereby, ERK activation.[73] *Drd*-DKO LSK cells show reduced phosphorylation of c-Kit after SCF treatment (Figure 6E). Conversely, treatment with 7-OH-DPAT and SCF significantly enhances c-Kit phosphorylation and ERK activation in LSK cells (Figure 6F-G).

Next, we investigated the underlying mechanism for the crosstalk between dopamine and ERK signaling. In different cell types, G protein–coupled receptors were found to transactivate receptor tyrosine kinases through mechanisms involving matrix metalloproteinases or β-arrestin.[75,76] However, inhibition of matrix metalloproteinases with marimastat or inhibition of β-arrestin with barbadin has no significant effect on ERK phosphorylation in LSK cells (supplemental Figure 7H). Src family kinases (SFKs) are also known activators of ERK signaling, and treatment of LSK cells with the SFK inhibitor PP2 significantly downregulates ERK pathway protein phosphorylation (supplemental Figure 7I-J). Our RNA-seq analysis shows that *Lck* mRNA, encoding the SFK Lck,[77] is highly expressed in LSK cells (Figure 6H; supplemental Figure 7K-L).[78] Furthermore, Lck mRNA and protein are downregulated in *Drd*-DKO and haloperidol-treated LSK cells (Figure 6I; supplemental Figure 7M), whereas 7-OH-DPAT increases Lck protein expression (Figure 6J). Treatment of LSK cells with the specific Lck inhibitor A-770041, which has a much lower affinity for c-Src or Fyn,[79] results in significantly decreased SCF-induced c-Kit phosphorylation and ERK activation (Figure 6K-M), whereas total ERK, MEK, and Raf are not significantly changed (supplemental Figure 7N). A-770041 treatment also results in lower BM transplantation efficiency, reduced EdU incorporation into donor cells in vivo, and impaired CFU formation ex vivo (Figure 6N-O; supplemental Figure 7O).

Next, we used lentiviruses to express short hairpin RNAs against *Lck* (*shLck*) in mouse cells (supplemental Figure 8A). Infection of LSK cells with *shLck* results in significant downregulation of Lck protein and reduced ERK phosphorylation (Figure 7A-B). Similar to A-770041 treatment, *shLck*-infected LSK cells show a significant reduction in colony formation ability and lower BM transplantation efficiency (Figure 7C; supplemental Figure 8B-D). Conversely, lentiviral overexpression of *Lck* results in higher Lck protein levels and ERK phosphorylation in *Drd*-DKO LSK cells (DKO+*Lck*) relative to control virus (DKO+*GFP*) (Figure 7D-E). Furthermore, the strong increase in SCF-induced ERK phosphorylation seen after Lck overexpression is abolished by knockdown of c-Kit (supplemental Figure 8E-F). In serial CFU assays, DKO+*Lck* cells show increased colony formation ability and absolute cell numbers (Figure 7F; supplemental Figure 8G-I). Although transplantation of DKO+*GFP* cells into lethally irradiated WT recipients leads to substantial lethality at 7 to 10 days after irradiation, no lethality is seen with the same number of DKO+*Lck* donor cells within this time period (Figure 7G-H). DKO+*Lck*-transplanted mice show significantly higher numbers of BMNCs and LSK cells, higher percentages of LSK and $CD45^+$ cells, and increased LSK cell proliferation, as shown by EdU incorporation and Ki67 expression (Figure 7I-K). Thus, Lck overexpression can partially rescue key aspects of the *Drd*-DKO phenotype, consistent with Lck acting downstream of D_2-type dopamine receptors in LSK cells.

Finally, we investigated how Lck is regulated by D_2-type dopamine receptors, which suppress cyclic adenosine monophosphate (cAMP)/protein kinase A (PKA) signaling in response to ligand binding.[80] Treatment of WT and *Drd*-DKO LSK cells ex vivo with the PKA inhibitor H-89 upregulates expression of Lck (Figure 7L; supplemental Figure 8J). H-89 treatment enhances SCF-induced ERK phosphorylation in LSK cells (Figure 7M). Conversely, treatment of LSK cells with forskolin, which activates cAMP/PKA activity by stimulation of adenylate cyclase, downregulates Lck expression, as well as SCF-induced ERK phosphorylation (Figure 7N). These results argue for the involvement of cAMP/PKA signaling in the regulation of Lck by dopamine.

Downloaded from http://ashpublications.net/blood/article-pdf/138/21/2051/1868550/bloodbld2020010419.pdf by guest on 29 May 2024

Together, our results indicate that Lck, regulated by dopamine signaling, controls ERK activation in LSK cells with important implications for c-Kit signaling and HSPC function.

Discussion

Based on the sum of our findings, we propose that dopamine in BM directly controls the homeostasis, proliferation, gene expression, and function of HSPCs through activation of D_2-type dopamine receptors. Mechanistically, dopamine controls the expression of the kinase Lck,[77,81] which, in turn, is required for activation of ERK signaling by c-Kit in response to SCF. In neurons and other cell types known to express D_2-type receptors, transcripts are present at low levels so that positive cells are rare or absent in many single-cell RNA-seq data sets (supplemental Figure 9). However, low expression of D_2-type receptor mRNA is sufficient to generate functional protein in neurons.[63] Therefore, we have validated expression of Drd2 and Drd3 in LSK cells and HSCs using multiple independent approaches, including qPCR, *Drd2-GFP* reporter mice, flow cytometry, and immunostaining with the inclusion of *Drd*-DKO negative controls. These findings, together with our functional data, strongly argue for a cell-autonomous role for D_2-type receptors in HSPCs.

Lck is involved in T-cell function and signal transduction downstream of c-Kit in cancer cells but is also expressed in LSK cells (supplemental Figure 7K-L).[77,78,82–85] Vascular niches in BM are major sources of SCF, which controls HSC maintenance through activation of c-Kit.[13,15,20–23] The strength of c-Kit signaling is critical for HSC function, as demonstrated by hematopoietic defects in partial loss-of-function (white spotting) mutant mice.[31,86–88] The expression of Lck is changed in some clusters of HSPCs in *Kit*^{W41} mice based on analysis of single-cell RNA-seq data.[89] Previous work has shown that HSCs from all developmental stages present similar levels of c-Kit on the cell surface, despite substantial differences in sensitivity to SCF between, for example, fetal and adult HSCs.[90] Such differences might be intrinsically preprogrammed but could also reflect a role for dopamine signaling and the modulation of Lck expression levels. Interestingly, there are results suggesting that SCF can act synergistically with other factors in human mast cells or prostate cancer cells.[91,92] Based on our results, we propose that c-Kit activation and downstream signaling in LSK cells are influenced by dopamine. Considering that SCF and dopamine are provided by different cellular sources, this implies that c-Kit signaling in HSPCs is regulated by a combination of different external signals and not only by the local concentration of SCF alone.

Our work highlights the importance of D_2-type dopamine receptors in the healthy and challenged hematopoietic system. Future research will explore whether therapeutic activation of D_2-type dopamine receptors might be beneficial to preserve or enhance the functionality of the hematopoietic system in disease or after transplantation.

Acknowledgments

This work was supported by the Max Planck Society, the University of Münster, the Deutsche Forschungsgemeinschaft cluster of excellence "Cells in Motion," the Leducq Foundation, and the European Research Council (AdG 786672, PROVEC). Y.L. was supported by Christiane Nüsslein-Volhard Stiftung.

Authorship

Contribution: R.H.A. designed research, interpreted data, and wrote the manuscript; Y.L. and Q.C. designed research, performed research, analyzed and interpreted data, and wrote the manuscript; H.-W.J. performed statistical analyses; J.F., H.D., and M.S. performed research; and D.H. and H.R.S. contributed vital new reagents.

Conflict-of-interest disclosure: The authors declare no competing financial interests.

ORCID profiles: Y.L., 0000-0002-4989-2404; Q.C., 0000-0001-8485-6540; H-W.J., 0000-0002-6976-6739; D.H., 0000-0002-8619-1543; J.F., 0000-0001-9673-5527; H.D., 0000-0002-8285-0644; H.R.S., 0000-0003-2643-5136; R.H.A., 0000-0003-3031-7677.

Correspondence: Ralf H. Adams, Department of Tissue Morphogenesis, Max-Planck-Institute for Molecular Biomedicine and University of Münster, Roentgenstrasse 20, D-48149 Münster, Germany; e-mail: ralf.adams@mpi-muenster.mpg.de.

Footnotes

Submitted 14 December 2020; accepted 25 July 2021; prepublished online on *Blood* First Edition 9 August 2021. DOI 10.1182/blood.2020010419.

*Y.L. and Q.C. contributed equally to this study.

The data reported in this article have been deposited in the Gene Expression Omnibus (accession numbers GSE134444 and GSE126219).

Data sharing requests should be sent to Ralf H. Adams (ralf.adams@mpi-muenster.mpg.de).

The full-text version of this article contains a data supplement.

There is a *Blood* Commentary on this article in this issue.

The publication costs of this article were defrayed in part by page charge payment. Therefore, and solely to indicate this fact, this article is hereby marked "advertisement" in accordance with 18 USC section 1734.

Downloaded from http://ashpublications.net/blood/article-pdf/138/21/2051/1868550/bloodbld2020010419.pdf by guest on 29 May 2024

REFERENCES

1. Hoggatt J, Kfoury Y, Scadden DT. Hematopoietic stem cell niche in health and disease. *Annu Rev Pathol*. 2016;11(1):555-581.
2. Pinho S, Frenette PS. Haematopoietic stem cell activity and interactions with the niche. *Nat Rev Mol Cell Biol*. 2019;20(5):303-320.
3. Morrison SJ, Scadden DT. The bone marrow niche for haematopoietic stem cells. *Nature*. 2014;505(7483):327-334.
4. Seita J, Weissman IL. Hematopoietic stem cell: self-renewal versus differentiation. *Wiley Interdiscip Rev Syst Biol Med*. 2010;2(6):640-653.
5. Frodermann V, Rohde D, Courties G, et al. Exercise reduces inflammatory cell production and cardiovascular inflammation via instruction of hematopoietic progenitor cells. *Nat Med*. 2019;25(11):1761-1771.
6. Poller WC, Nahrendorf M, Swirski FK. Hematopoiesis and cardiovascular disease. *Circ Res*. 2020;126(8):1061-1085.
7. Itkin T, Gur-Cohen S, Spencer JA, et al. Distinct bone marrow blood vessels differentially regulate haematopoiesis [published correction appears in *Nature*. 2016;538:274]. *Nature*. 2016;532(7599):323-328.
8. Crane GM, Jeffery E, Morrison SJ. Adult haematopoietic stem cell niches. *Nat Rev Immunol*. 2017;17(9):573-590.
9. Tikhonova AN, Dolgalev I, Hu H, et al. The bone marrow microenvironment at

single-cell resolution. *Nature*. 2019; 569(7755):222-228.

10. Baryawno N, Przybylski D, Kowalczyk MS, et al. A cellular taxonomy of the bone marrow stroma in homeostasis and leukemia. Cell. 2019;177(7):1915-1932.e6.

11. Méndez-Ferrer S, Scadden DT, Sánchez-Aguilera A. Bone marrow stem cells: current and emerging concepts. *Ann N Y Acad Sci*. 2015;1335(1):32-44.

12. Méndez-Ferrer S, Michurina TV, Ferraro F, et al. Mesenchymal and haematopoietic stem cells form a unique bone marrow niche. *Nature*. 2010;466(7308):829-834.

13. Zhou BO, Yu H, Yue R, et al. Bone marrow adipocytes promote the regeneration of stem cells and haematopoiesis by secreting SCF. *Nat Cell Biol*. 2017; 19(8):891-903.

14. Zhao M, Perry JM, Marshall H, et al. Megakaryocytes maintain homeostatic quiescence and promote post-injury regeneration of hematopoietic stem cells. *Nat Med*. 2014;20(11):1321-1326.

15. Chen Q, Liu Y, Jeong HW, et al. Apelin^{+} endothelial niche cells control hematopoiesis and mediate vascular regeneration after myeloablative injury. *Cell Stem Cell*. 2019; 25(6):768-783.e6.

16. Waclawiczek A, Hamilton A, Rouault-Pierre K, et al. Mesenchymal niche remodeling impairs hematopoiesis via stanniocalcin 1 in acute myeloid leukemia. *J Clin Invest*. 2020; 130(6):3038-3050.

17. Forte D, García-Fernández M, Sánchez-Aguilera A, et al. Bone marrow mesenchymal stem cells support acute myeloid leukemia bioenergetics and enhance antioxidant defense and escape from chemotherapy. *Cell Metab*. 2020; 32(5):829-843.e9.

18. Hoyer FF, Zhang X, Coppin E, et al. Bone marrow endothelial cells regulate myelopoiesis in diabetes mellitus. *Circulation*. 2020;142(3):244-258.

19. Mende N, Jolly A, Percin GI, et al. Prospective isolation of nonhematopoietic cells of the niche and their differential molecular interactions with HSCs. *Blood*. 2019;134(15):1214-1226.

20. Ding L, Saunders TL, Enikolopov G, Morrison SJ. Endothelial and perivascular cells maintain haematopoietic stem cells. *Nature*. 2012;481(7382):457-462.

21. Asada N, Kunisaki Y, Pierce H, et al. Differential cytokine contributions of perivascular haematopoietic stem cell niches. *Nat Cell Biol*. 2017; 19(3):214-223.

22. Xu C, Gao X, Wei Q, et al. Stem cell factor is selectively secreted by arterial endothelial cells in bone marrow. *Nat Commun*. 2018; 9(1):2449.

23. Comazzetto S, Murphy MM, Berto S, Jeffery E, Zhao Z, Morrison SJ. Restricted hematopoietic progenitors and erythropoiesis require SCF from leptin receptor+ niche cells in the bone marrow. *Cell Stem Cell*. 2019;24(3):477-486.e6.

24. Himburg HA, Termini CM, Schlussel L, et al. Distinct bone marrow sources of pleiotrophin control hematopoietic stem cell maintenance and regeneration. *Cell Stem Cell*. 2018;23(3):370-381.e5.

25. Guo P, Poulos MG, Palikuqi B, et al. Endothelial jagged-2 sustains hematopoietic stem and progenitor reconstitution after myelosuppression. *J Clin Invest*. 2017; 127(12):4242-4256.

26. Itkin T, Kumari A, Schneider E, et al. MicroRNA-155 promotes G-CSF-induced mobilization of murine hematopoietic stem and progenitor cells via propagation of CXCL12 signaling. *Leukemia*. 2017; 31(5):1247-1250.

27. Morgan RA, Gray D, Lomova A, Kohn DB. Hematopoietic stem cell gene therapy: progress and lessons learned. *Cell Stem Cell*. 2017;21(5):574-590.

28. Kondo M, Wagers AJ, Manz MG, et al. Biology of hematopoietic stem cells and progenitors: implications for clinical application. *Annu Rev Immunol*. 2003; 21(1):759-806.

29. Méndez-Ferrer S, Bonnet D, Steensma DP, et al. Bone marrow niches in haematological malignancies. *Nat Rev Cancer*. 2020; 20(5):285-298.

30. Batsivari A, Haltalli MLR, Passaro D, Pospori C, Lo Celso C, Bonnet D. Dynamic responses of the haematopoietic stem cell niche to diverse stresses [published correction appears in *Nat Cell Biol*. 2020;22:257]. *Nat Cell Biol*. 2020;22(1):7-17.

31. Cosgun KN, Rahmig S, Mende N, et al. Kit regulates HSC engraftment across the human-mouse species barrier. *Cell Stem Cell*. 2014;15(2):227-238.

32. Copelan EA. Hematopoietic stem-cell transplantation. *N Engl J Med*. 2006; 354(17):1813-1826.

33. Méndez-Ferrer S, Lucas D, Battista M, Frenette PS. Haematopoietic stem cell release is regulated by circadian oscillations. *Nature*. 2008;452(7186):442-447.

34. Golan K, Kumari A, Kollet O, et al. Daily onset of light and darkness differentially controls hematopoietic stem cell differentiation and maintenance. *Cell Stem Cell*. 2018;23(4):572-585.e7.

35. Sugiyama T, Kohara H, Noda M, Nagasawa T. Maintenance of the hematopoietic stem cell pool by CXCL12-CXCR4 chemokine signaling in bone marrow stromal cell niches. *Immunity*. 2006;25(6):977-988.

36. García-García A, Korn C, García-Fernández M, et al. Dual cholinergic signals regulate daily migration of hematopoietic stem cells and leukocytes [published correction appears in *Blood*. 2020;136(25):2965]. *Blood*. 2019;133(3):224-236.

37. Lucas D, Bruns I, Battista M, et al. Norepinephrine reuptake inhibition promotes mobilization in mice: potential impact to rescue low stem cell yields. *Blood*. 2012;119(17):3962-3965.

38. Golan K, Kollet O, Markus RP, Lapidot T. Daily light and darkness onset and circadian rhythms metabolically synchronize hematopoietic stem cell differentiation and maintenance: the role of bone marrow norepinephrine, tumor necrosis factor, and melatonin cycles. *Exp Hematol*. 2019; 78:1-10.

39. Fielding C, Méndez-Ferrer S. Neuronal regulation of bone marrow stem cell niches. *F1000 Res*. 2020;9:614.

40. Lucas D, Scheiermann C, Chow A, et al. Chemotherapy-induced bone marrow nerve injury impairs hematopoietic regeneration. *Nat Med*. 2013;19(6):695-703.

41. Arranz L, Sánchez-Aguilera A, Martín-Pérez D, et al. Neuropathy of haematopoietic stem cell niche is essential for myeloproliferative neoplasms. *Nature*. 2014;512(7512):78-81.

42. Maryanovich M, Zahalka AH, Pierce H, et al. Adrenergic nerve degeneration in bone marrow drives aging of the hematopoietic stem cell niche [published correction appears in *Nat Med*. 2019;24(4):701]. *Nat Med*. 2018;24(6):782-791.

43. Hanoun M, Zhang D, Mizoguchi T, et al. Acute myelogenous leukemia-induced sympathetic neuropathy promotes malignancy in an altered hematopoietic stem cell niche. *Cell Stem Cell*. 2014;15(3):365-375.

44. Ho YH, Del Toro R, Rivera-Torres J, et al. Remodeling of bone marrow hematopoietic stem cell niches promotes myeloid cell expansion during premature or physiological aging. *Cell Stem Cell*. 2019; 25(3):407-418.e6.

45. Maryanovich M, Takeishi S, Frenette PS. Neural regulation of bone and bone marrow. *Cold Spring Harb Perspect Med*. 2018;8(9):a031344.

46. Mendelson A, Frenette PS. Hematopoietic stem cell niche maintenance during homeostasis and regeneration. *Nat Med*. 2014;20(8):833-846.

47. Daubner SC, Le T, Wang S. Tyrosine hydroxylase and regulation of dopamine synthesis. *Arch Biochem Biophys*. 2011; 508(1):1-12.

48. Schultz W. Multiple dopamine functions at different time courses. *Annu Rev Neurosci*. 2007;30(1):259-288.

49. Warren N, O'Gorman C, Lehn A, Siskind D. Dopamine dysregulation syndrome in Parkinson's disease: a systematic review of published cases. *J Neurol Neurosurg Psychiatry*. 2017;88(12):1060-1064.

50. Beaulieu JM, Gainetdinov RR. The physiology, signaling, and pharmacology of dopamine receptors. *Pharmacol Rev*. 2011; 63(1):182-217.

51. Lindeberg J, Usoskin D, Bengtsson H, et al. Transgenic expression of Cre recombinase from the tyrosine hydroxylase locus. *Genesis*. 2004;40(2):67-73.

Downloaded from http://ashpublications.net/blood/article-pdf/138/21/2051/1868550/bloodbld2020010419.pdf by guest on 29 May 2024

52. Buch T, Heppner FL, Tertilt C, et al. A Cre-inducible diphtheria toxin receptor mediates cell lineage ablation after toxin administration. *Nat Methods*. 2005;2(6):419-426.

53. Kelly MA, Rubinstein M, Asa SL, et al. Pituitary lactotroph hyperplasia and chronic hyperprolactinemia in dopamine D2 receptor-deficient mice. *Neuron*. 1997;19(1):103-113.

54. Accili D, Fishburn CS, Drago J, et al. A targeted mutation of the D3 dopamine receptor gene is associated with hyperactivity in mice. *Proc Natl Acad Sci USA*. 1996;93(5):1945-1949.

55. Muzumdar MD, Tasic B, Miyamichi K, Li L, Luo L. A global double-fluorescent Cre reporter mouse. *Genesis*. 2007; 45(9):593-605.

56. de Boer J, Williams A, Skavdis G, et al. Transgenic mice with hematopoietic and lymphoid specific expression of Cre. *Eur J Immunol*. 2003;33(2):314-325.

57. Danielian PS, Muccino D, Rowitch DH, Michael SK, McMahon AP. Modification of gene activity in mouse embryos in utero by a tamoxifen-inducible form of Cre recombinase. *Curr Biol*. 1998;8(24):1323-1326.

58. DeFalco J, Tomishima M, Liu H, et al. Virus-assisted mapping of neural inputs to a feeding center in the hypothalamus. *Science*. 2001;291(5513):2608-2613.

59. Doyle JP, Dougherty JD, Heiman M, et al. Application of a translational profiling approach for the comparative analysis of CNS cell types. *Cell*. 2008;135(4):749-762.

60. Spiegel A, Shivtiel S, Kalinkovich A, et al. Catecholaminergic neurotransmitters regulate migration and repopulation of immature human CD34+ cells through Wnt signaling. *Nat Immunol*. 2007;8(10):1123-1131.

61. Azevedo EP, Pomeranz L, Cheng J, et al. A role of Drd2 hippocampal neurons in context-dependent food intake. *Neuron*. 2019;102(4):873-886.e5.

62. Zhang Y, Chen K, Sloan SA, et al. An RNA-sequencing transcriptome and splicing database of glia, neurons, and vascular cells of the cerebral cortex. *J Neurosci*. 2014; 34(36):11929-11947.

63. Surmeier DJ, Song WJ, Yan Z. Coordinated expression of dopamine receptors in neostriatal medium spiny neurons. *J Neurosci*. 1996;16(20):6579-6591.

64. Bourne JA. SCH 23390: the first selective dopamine D1-like receptor antagonist. *CNS Drug Rev*. 2001;7(4):399-414.

65. Leyden E, Tadi P. Carbidopa. Treasure Island, FL: StatPearls; 2020.

66. Flach J, Bakker ST, Mohrin M, et al. Replication stress is a potent driver of functional decline in ageing haematopoietic stem cells. *Nature*. 2014;512(7513):198-202.

67. Olsson R, Remberger M, Schaffer M, et al. Graft failure in the modern era of allogeneic hematopoietic SCT [published correction appears in *Bone Marrow Transplant*. 2013;48(4):616]. *Bone Marrow Transplant*. 2013;48(4):537-543.

68. Penack O, Peczynski C, Mohty M, et al. How much has allogeneic stem cell transplant-related mortality improved since the 1980s? A retrospective analysis from the EBMT. *Blood Adv*. 2020;4(24):6283-6290.

69. Chambard JC, Lefloch R, Pouysségur J, Lenormand P. ERK implication in cell cycle regulation. *Biochim Biophys Acta*. 2007; 1773(8):1299-1310.

70. Mebratu Y, Tesfaigzi Y. How ERK1/2 activation controls cell proliferation and cell death: is subcellular localization the answer? *Cell Cycle*. 2009;8(8):1168-1175.

71. Chan G, Gu S, Neel BG. Erk1 and Erk2 are required for maintenance of hematopoietic stem cells and adult hematopoiesis. *Blood*. 2013;121(18):3594-3598.

72. Baumgartner C, Toifl S, Farlik M, et al. An ERK-dependent feedback mechanism prevents hematopoietic stem cell exhaustion. *Cell Stem Cell*. 2018;22(6):879-892.e6.

73. Thömmes K, Lennartsson J, Carlberg M, Rönnstrand L. Identification of Tyr-703 and Tyr-936 as the primary association sites for Grb2 and Grb7 in the c-Kit/stem cell factor receptor. *Biochem J*. 1999; 341(Pt 1):211-216.

74. Wandzioch E, Edling CE, Palmer RH, Carlsson L, Hallberg B. Activation of the MAP kinase pathway by c-Kit is PI-3 kinase dependent in hematopoietic progenitor/stem cell lines. *Blood*. 2004;104(1):51-57.

75. Shah BH, Catt KJ. GPCR-mediated transactivation of RTKs in the CNS: mechanisms and consequences. *Trends Neurosci*. 2004;27(1):48-53.

76. Jean-Charles PY, Kaur S, Shenoy SKG. G protein-coupled receptor signaling through β-arrestin-dependent mechanisms. *J Cardiovasc Pharmacol*. 2017;70(3):142-158.

77. Gaud G, Lesourne R, Love PE. Regulatory mechanisms in T cell receptor signalling. *Nat Rev Immunol*. 2018;18(8):485-497.

78. Nestorowa S, Hamey FK, Pijuan Sala B, et al. A single-cell resolution map of mouse hematopoietic stem and progenitor cell differentiation. *Blood*. 2016;128(8):e20-e31.

79. Burchat A, Borhani DW, Calderwood DJ, Hirst GC, Li B, Stachlewitz RF. Discovery of A-770041, a src-family selective orally active lck inhibitor that prevents organ allograft rejection. *Bioorg Med Chem Lett*. 2006; 16(1):118-122.

80. Bonci A, Hopf FW. The dopamine D2 receptor: new surprises from an old friend. *Neuron*. 2005;47(3):335-338.

81. Bommhardt U, Schraven B, Simeoni L. Beyond TCR signaling: emerging functions of Lck in cancer and immunotherapy. *Int J Mol Sci*. 2019;20(14):3500.

82. Courtney AH, Lo WL, Weiss A. TCR signaling: mechanisms of initiation and propagation. *Trends Biochem Sci*. 2018; 43(2):108-123.

83. Omri B, Crisanti P, Marty MC, et al. The Lck tyrosine kinase is expressed in brain neurons. *J Neurochem*. 1996; 67(4):1360-1364.

84. Bondzi C, Litz J, Dent P, Krystal GW. Src family kinase activity is required for Kit-mediated mitogen-activated protein (MAP) kinase activation, however loss of functional retinoblastoma protein makes MAP kinase activation unnecessary for growth of small cell lung cancer cells. *Cell Growth Differ*. 2000;11(6):305-314.

85. Krystal GW, DeBerry CS, Linnekin D, Litz J. Lck associates with and is activated by Kit in a small cell lung cancer cell line: inhibition of SCF-mediated growth by the Src family kinase inhibitor PP1. *Cancer Res*. 1998; 58(20):4660-4666.

86. Thorén LA, Liuba K, Bryder D, et al. Kit regulates maintenance of quiescent hematopoietic stem cells. *J Immunol*. 2008; 180(4):2045-2053.

87. Nocka K, Tan JC, Chiu E, et al. Molecular bases of dominant negative and loss of function mutations at the murine c-kit/white spotting locus: W37, Wv, W41 and W. *EMBO J*. 1990;9(6):1805-1813.

88. Waskow C, Paul S, Haller C, Gassmann M, Rodewald HR. Viable c-Kit(W/W) mutants reveal pivotal role for c-kit in the maintenance of lymphopoiesis. *Immunity*. 2002; 17(3):277-288.

89. Dahlin JS, Hamey FK, Pijuan-Sala B, et al. A single-cell hematopoietic landscape resolves 8 lineage trajectories and defects in Kit mutant mice. *Blood*. 2018;131(21):e1-e11.

90. Kent D, Copley M, Benz C, Dykstra B, Bowie M, Eaves C. Regulation of hematopoietic stem cells by the steel factor/KIT signaling pathway. *Clin Cancer Res*. 2008; 14(7):1926-1930.

91. Ma Y, Liang D, Liu J, et al. Synergistic effect of SCF and G-CSF on stem-like properties in prostate cancer cell lines. *Tumour Biol*. 2012;33(4):967-978.

92. Tsang CM, Wong CK, Ip WK, Lam CW. Synergistic effect of SCF and TNF-alpha on the up-regulation of cell-surface expression of ICAM-1 on human leukemic mast cell line (HMC)-1 cells. *J Leukoc Biol*. 2005; 78(1):239-247.

Downloaded from http://ashpublications.net/blood/article-pdf/138/21/2051/1868550/bloodbld2020010419.pdf by guest on 29 May 2024